Valence-core self-consistency in the $A = 17$ system

J. P. Vary and R. H. Belehrad
Ames Laboratory-DOE and Department of Physics, Iowa State University, Ames, Iowa 50011

R. J. McCarthy
Kent State University, Ashtabula Campus, Ashtabula, Ohio 44004*
and Ames Laboratory-DOE, Iowa State University, Ames, Iowa 50011

(Received 27 August 1979)

We develop a systematic approach to the calculation of self-consistency effects in core plus valence nucleon systems. A detailed calculation of the effective one-body Hamiltonian for $A = 17$ in an $11\hbar\Omega$ model space is readily extrapolated to a $20\hbar\Omega$ model space which is sufficient to develop accurate tails for the single-particle wave functions. The effective one-body interaction is found using a Brillouin-Wigner type perturbation theory which eliminates folded diagrams and leads to a manifestly Hermitian interaction. A renormalized Brueckner calculation is performed for $A = 16$ and the results are employed in a shell-model study of $A = 17$. The self-consistent results still have a weak dependence on the initial unperturbed Hamiltonian. However, we find a single unperturbed Hamiltonian which yields a reasonable binding energy for $A = 16$ and, except for a weak spin-orbit splitting, reasonable results for the lowest states in the $A = 17$ system. This agreement is important for continued valence s-d shell studies.

[NUCLEAR STRUCTURE Brueckner theory, self-consistency effects, ^{17}O spectra and wave functions, ^{16}O properties.]

I. INTRODUCTION

Since the pioneering studies of microscopically derived effective nuclear shell-model Hamiltonians in the mid-1960's,[1] much attention has been devoted to assessing the role of corrections. Primary interest has centered on the order-by-order convergence (in the Brueckner reaction G matrix),[2] the convergence of intermediate state sums,[3] and the role of self-consistency effects.[4,5] The results indicate that all three problems provide major hurdles for the perturbation approach based on the G matrix. We develop a systematic approach to the particle-core case in order to establish a consistent but flexible framework, incorporating self-consistency effects in a large model space, for an eventual study of the multinucleon shell-model problem.

A number of previous investigations[4,5] have demonstrated that self-consistency effects on valence orbits can be quite large even in light nuclei, and when included to high orders, can substantially alter contributions to the multinucleon effective shell-model interaction. Primarily, these results have been obtained for the $A = 17$ and $A = 18$ systems in a $2\hbar\Omega$ model space where the valence particles are initially in an oscillator basis. The main differences among previous studies seem to be the choice of diagrams to include as "self-consistency" effects and whether single-particle energies and wave functions are both corrected or just the energies.

From these earlier works, we draw two important conclusions that motivate the present efforts. First, self-consistency effects are large and defy approximate or low-order treatments. Second, when included, the self-consistency effects dramatically reduce higher order effective shell-model interaction diagrams and improve the rate of convergence of the linked cluster expansion.

The major emphasis of the present effort is to solve the $A = 17$ problem in a large valence space using a realistic nucleon-nucleon interaction in order to develop self-consistent single-particle energies and wave functions. These results will be employed in later studies of electromagnetic properties of $A = 17$ and in eventual multinucleon studies in the sd shell.

A secondary interest in the present study, is to obtain a single choice of the unperturbed Hamiltonian such that the results for the effective Hamiltonians (through second order in G) are in agreement with experiment for the $A = 16$ *and* $A = 17$ systems. This addresses the question of whether, even with inadequacies in our current realistic nucleon-nucleon potentials, we might nevertheless achieve reasonably good descriptions of the valence properties of nuclei.

Section II contains a brief review of the linked cluster expansion for a single particle outside a closed core in an unperturbed representation. In addition, we outline the expansion for the situation where a renormalized Brueckner (RB) calculation is performed for the core state. We then show in the most complete calculations performed here how the valence and core states are treated con-

sistently in an RB and shell-model diagonalization.

In Sec. III we introduce the model space, interaction, G-matrix, Pauli operator, and representation selections. Section IV contains the results, a discussion, and conclusions.

II. SINGLE-PARTICLE EFFECTIVE SHELL-MODEL HAMILTONIANS

Here, we introduce a progression of effective Hamiltonians in order to display the methods we employ that systematically include larger classes of diagrams. We develop these Hamiltonians specifically for a large model space ($11\hbar\Omega$ initially) in order that valence self-consistency effects and converged intermediate state summations may be included. Later we extrapolate the effective Hamiltonian to a $20\hbar\Omega$ space to achieve accurate tails of single-particle wave functions.

Within the Bloch-Horowitz-Brandow theory of the effective shell-model interaction we solve for

$$H^v_{eff}\,|\Psi^v_i\rangle=\epsilon_i\,|\Psi^v_i\rangle\,, \tag{1}$$

where the superscript v denotes quantities defined within the valence space. Furthermore, $|\Psi^v_i\rangle$ is defined as the projection of the exact eigenfunction of the full Hamiltonian on to the valence space. The effective Hamiltonian is composed of an unperturbed one-body part H^v_0 which, in principle, is arbitrary and a residual effective interaction V_{eff} given by the linked cluster expansion in terms of the Brueckner reaction matrix G. For the $A=17$ nucleus, the effective interaction is also a one-body operator and henceforward we refer to it as U_{eff}. A complete set of linked diagrams for U_{eff} through third order in G has been given by Kassis.[6] For handy reference and for purposes of assigning convenient labels we show the series through second order in Fig. 1.

Wavy lines represent G-matrix elements where G is given by the standard form

$$G(\omega)=V+V\frac{Q}{\omega-H_0(\gamma)}G(\omega)\,. \tag{2}$$

Here V is the nucleon-nucleon interaction determined by fitting the two-nucleon data, Q is the two particle Pauli operator preventing scattering to those intermediate states that are normally occupied or to those two particle intermediate states in the model space. The parameter ω specifies the G-matrix starting energy appropriate to the position of G in the diagram. A detailed presentation of the method used to solve for the G matrix exactly in a harmonic oscillator single-particle basis has been given in Ref. 7.

The unperturbed one-body Hamiltonian H^v_0 has been expressed as $H_0(\gamma)$ in Eq. (2) where γ indicates the set of parameters specifying H^v_0. These parameters are discussed in detail in Sec. III. U_{eff} depends on $H_0(\gamma)$ in a number of ways. The diagrams shown in Fig. 1 contain $U_0(\gamma)$ insertions [where $H_0(\gamma)=T+U_0(\gamma)$] which are indicated by the X's within the bubbles. U_{eff} depends on $H_0(\gamma)$ through G, and all intermediate state energy denominators depend on $H_0(\gamma)$.

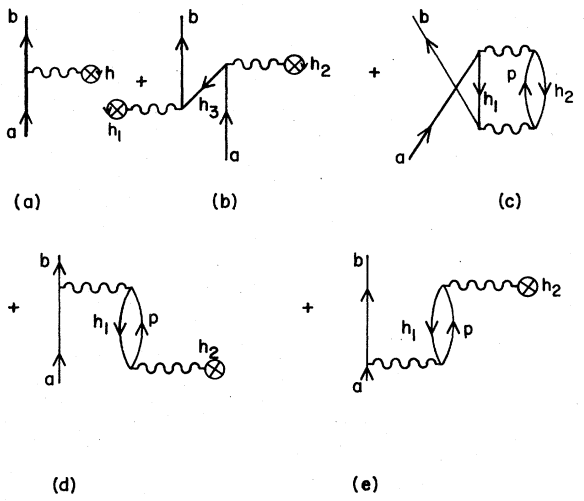

FIG. 1. Lowest order single-particle potential diagrams included in the diagonalization. The x's in the bubbles represent $-U_0$ insertions. In the SM calculation all single-particle energies are defined by $H_0(\gamma)$. In the RBSM calculation the hole energies are obtained from a self-consistent calculation of ^{16}O and all bubbles are multiplied by occupation probabilities.

The intermediate state energies, including those hidden in G, also depend upon the diagram starting energy which is determined by the form chosen for the perturbation expansion. This starting energy E^v_0 is usually chosen as the unperturbed energy of the valence particle entering the diagram. This choice of E^v_0 leads to a folded diagram expansion and a non-Hermitian effective interaction.

On the other hand E^v_0 may be chosen self-consistently to equal the energy of the lowest eigenstate found in the diagonalization of the effective interaction. This choice yields a Brillouin-Wigner valence perturbation expansion and has usually been avoided in effective interaction calculations since it leads to unlinked valence diagrams. However, there can be no unlinked valence diagrams in the $A=17$ system, nor in the $A=18$ and $A=19$ systems if self-consistent valence orbitals are used in the calculations. In the calculations presented here we will use self-consistent E^v_0's for the $d_{5/2}$, $s_{1/2}$, and $d_{3/2}$ effective interactions.

It is instructive to carry out the calculation of H_{eff} at two different levels of self-consistency.

The first level consists of including only the diagrams of Fig. 1 and using $H_0(\gamma)$ to describe the core orbitals. This calculation, which treats only E_0^v self-consistently, we refer to as a (shell-model) (SM) calculation. The second level of calculation (RBSM) is obtained by carrying out a renormalized Brueckner (RB) calculation of the core and using self-consistent core results as input to the $A=17$ effective interaction calculation.

The RBSM calculations include explicitly only the diagrams of Fig. 1 with the additional features that all bubbles are multiplied by self-consistent occupation probabilities. However, the RBSM approach implicitly includes two additional classes of diagrams into the calculations. The first class of additional diagrams, obtained by using self-consistent hole energies, is indicated to low order in Fig. 2. In the first diagram of Fig. 2 we have opened up the G matrix of Fig. 1(a) to indicate the fact that the G-matrix elements themselves, as well as the intermediate energy denominators, are influenced by the use of self-consistent hole energies. The two other diagrams in Fig. 2 indicate some higher order terms which are implicitly included.

A second class of diagrams is included by utilizing the self-consistent occupation probabilities obtained in the $A=16$ calculation. All bubble insertions are multiplied by the occupation probability of the hole represented by the bubble. As shown in Fig. 3, this has the effect of replacing the bubble insertion by the sum of two insertions. Analytic expressions for all diagrams included in the core and valence calculations are given in the Appendix, along with additional details of the calculational procedure.

III. METHOD OF CALCULATION

We select the harmonic oscillator for H_0 and employ an overall shift V_0 and a boost C for the particle space for additional flexibility. Therefore

$$H_0(C, V_0) = H_{\rm osc} - V_0 + QCQ\,, \tag{3}$$

where Q projects on to the particle states. Thus, if we signify pure oscillator energies by

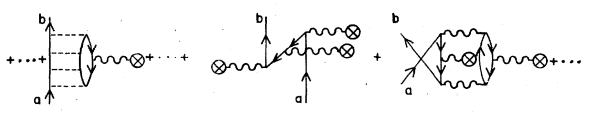

FIG. 2. Some low-order diagrams included by using self-consistent hole energies. The major effect arises from the starting energy dependence in the G matrix of Fig. 1 (a). This effect is indicated diagrammatically in the first diagram shown in this figure.

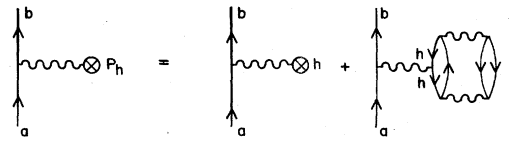

FIG. 3. Lowest order diagrams included by the use of self-consistent occupation probabilities in the RBSM framework.

$$e_a = (2n_a + l_a + \tfrac{3}{2})\hbar\Omega\,, \tag{4}$$

then $H_0(C, V_0)$ has a single-particle spectrum given by

$$\epsilon_h = e_h - V_0 \text{ for } h \text{ in } 0s \text{ and } 0p \text{ shells}, \tag{5}$$

$$\epsilon_p = e_p - (V_0 - C) \text{ for } p \text{ in } sd \text{ shell and above}. \tag{6}$$

We choose $\hbar\Omega = 14$ MeV. To illustrate the utility and motivation for choices of V_0 and C, we consider three cases depicted in Fig. 4. Column 1 displays the pure oscillator energies e_a whereas column 2 displays the spectrum with a physically sensible choice of V_0 that places the s and p shells

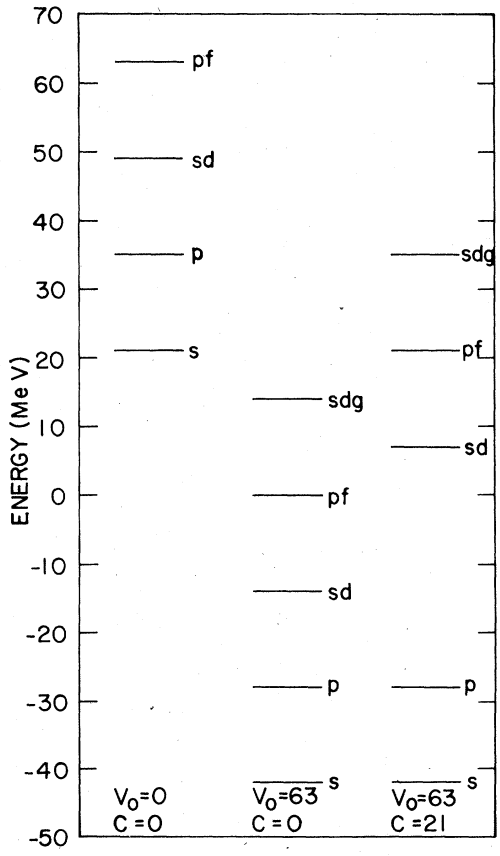

FIG. 4. Oscillator spectra ($\hbar\Omega = 14$ MeV) for three representative choices of the overall shift V_0 and the particle space boost C parameters.

near where we expect them to lie as a result of our calculations. The flexibility provided by C is exercised in column 3 to place the *sd* shell closer to where it would be if the average oscillator potential energy were removed (24.5 MeV). Thus C may be employed to account, in an average way, for the desire to place low-lying unoccupied oscillator orbits near their average kinetic energy values and thus diminish the oscillator potential in these states.

We wish to emphasize two points here. First, a converged calculation of the properties of ^{16}O and ^{17}O will be independent of V_0 and C. Dependence on V_0 and C in the physically sensible region described above will be studied here as a gauge of our approach to convergence. Second, since convergence is not fully achieved we will employ the *same* H_0 in the calculations for the binding energy of ^{16}O and for the valence properties of ^{17}O. It is planned that this consistency will be maintained for studies of other valence systems. An important feature of the RBSM calculation, with its self-consistent treatment of both core and valence single-particle energies, is that the results depend only on the absolute energies of the remaining particle states. Hence the RBSM results depend only on $V_0 - C$ and not independently on V_0 and C. This simplifies the presentation of results below. We have not made a study of the $\hbar\Omega$ dependence of our results.

To maintain the calculational effort within reasonable limits, we have elected to preserve the 0*s* and 0*p* orbits as pure oscillator states throughout this work. The corrections to these orbits are achieved through perturbation theory by adding the necessary diagrams to our study. Thus the diagrams in Figs. 1(b), 1(d), and 1(e) are nonzero. We find the contributions of these diagrams are quite small which is consistent with our perturbative approach. The valence orbits extend to all orbits beyond the core states. Thus we must diagonalize ^{17}O in increasing spaces in order to assess convergence with size of basis space. For some cases, convergence for energies of the lowest lying bound states is well achieved in a space spanned by five oscillator shells. The corresponding wave functions are converged out to approximately 6 fm. We describe techniques which allow us to extend our space to 10 major shells, which we feel is adequate for the present study since the bound state wave functions then have an exponential falloff out to 8 fm.

The G matrix is solved on a four point ω mesh ($\omega = 79$, 51, 23, -5 MeV) and numerical interpolation is employed to obtain the required intermediate values. The Pauli operator is of the Brueckner-Hartree-Fock type but simpler since the 0*s* and 0*p* states are maintained as pure oscillators. This Pauli operator is treated exactly, in a single-particle basis, according to the methods described in Ref. 7. The realistic nucleon-nucleon interaction here is the Reid soft-core potential.

IV. RESULTS

We present in Tables I and II the individual diagram contributions to the effective single-particle Hamiltonian. Results are presented for RBSM (first line of each n, n' row) and SM calculations with $V_0 - C = 48$ MeV and E_0^v chosen self-consistently. We note first that Fig. 1(b) does not contribute to the $d_{5/2}$ interaction and that Figs. 1(d) and 1(e) give very small contributions. These diagrams have a larger influence on the $s_{1/2}$ calculations but are obviously small enough so the approximation of treating core excitations in perturbation theory should be adequate.

The total diagram contribution to U_{eff} is shown in column 7. When added to $H_0(C, V_0)$ it gives the complete single-particle Hamiltonian H_{eff} which is then diagonalized to obtain self-consistent valence wave functions. It should be emphasized that only the lowest state of a given j is treated self-consistently since E_0^v is chosen to be equal to the lowest eigenvalue of the diagonalization. The total one-body Hamiltonian is normally expressed as

$$H_{eff} = H_0 + U_{eff}, \tag{7}$$

and this approach has been used to carry out our calculations where H_0 is a function of C and V_0. However, now that matrix elements of H are known we are free to use the alternate expression

$$H_{eff} = T + \overline{U}_{eff}. \tag{8}$$

Oscillator matrix elements of T and $\overline{U}_{eff}$ are shown in the last two columns of Tables I and II. The latter expression is particularly useful here since oscillator matrix elements of $\overline{U}_{eff}$ fall off in a regular fashion with increasing radial quantum number.

In Fig. 5 we show the behaviors of diagonal and nearest off-diagonal matrix elements of $\overline{U}_{eff}$ with increasing n. These matrix elements fall off exponentially. We extrapolate from $n = 5$ to $n = 10$ based on a fit to the last two calculated values. This extrapolation allows us to effectively expand our valence space to include 10 oscillator orbits of each symmetry (lj) and the numerical results below are based on diagonalizations in this larger space. The lowest eigenvalues are well converged in the 5 oscillator shell space but the tails of the resulting eigenvectors are greatly improved in the region between 6 fm and 8 fm by use of the expanded space.

Consider first the overall trends of the energies

in our results as shown in Figs. 6 and 7. The ground state energy per particle of ^{16}O is consistent with previous RBHF (Ref. 8) results as may be expected since we have argued that self-consistency of the core wave functions should provide minor differences from oscillator wave functions.

A striking feature of these results is the similarity of dependence of core and valence single-particle states in the RB and RBSM calculations on $V_0 - C$. Thus one is encouraged to believe that a similar degree of convergence has been achieved for core and valence energies in this approach. For the SM case, with its separate dependence on V_0 and C, the C dependence (fixed V_0) is somewhat stronger than the RBSM results. On the other hand, the V_0 dependence (fixed C) is somewhat weaker. Thus the SM convergence behavior seems to bracket that of the RBSM. For comparison we have shown in Fig. 6 the behavior of the unperturbed $d_{5/2}$ oscillator state as a function of $V_0 - C$. The contrast with the self-consistent results indicates the progress towards convergence.

An important aspect of the RBSM calculation was the role of choosing E_0^v self-consistently. This enhances the $E(d_{5/2})$ independence of $V_0 - C$. Since the core single-particle states are treated self-

TABLE I. H_{eff} $(d_{5/2})$. Contributions to the effective Hamiltonian matrix elements for the $d_{5/2}$ states of ^{17}O. The first row for each n, n' entry (bra and ket principal quantum numbers) are for the RBSM Hamiltonian with $V_0 - C = 48$ MeV and E_0^v chosen self-consistently as -3.0 MeV. The second row gives the SM effective Hamiltonian with $V_0 = 78$ MeV and $C = 30$ MeV while $E_0^v = -4.3$ MeV, the self-consistent choice. We use the convention that the numbers not listed are strictly zero, or are identical to the number immediately above since no confusion should arise.

				Diagram						
n	n'	G insertion	$-U_0$ insertion	1(b)	1(c)	1($d+e$)	U_{eff}	H_{eff}	T	$\bar{U}_{\text{eff}}$
0	0	−28.02	23.50		1.17	−0.13	−3.48	−2.48	24.50	−26.98
		−29.05			0.72	−0.14	−4.97	−3.97		−28.47
0	1	−12.36	13.10		0.58	−0.31	1.00	1.00	13.10	−12.10
		−13.38			0.43	−0.23	−0.08	−0.08		−13.18
0	2	−3.07			0.32	−0.21	−2.96	−2.96		−2.96
		−3.56			0.27	−0.14	−3.43	−3.43		−3.43
0	3	0.04			0.19	−0.03	0.20	0.20		0.20
		0.07			0.17	−0.01	0.09	0.09		0.09
0	4	0.50			−0.08	0.09	0.51	0.51		0.51
		0.55			−0.06	0.08	0.57	0.57		0.57
1	1	−15.33	9.50		0.56	−0.10	−5.36	23.64	38.50	−14.86
		−16.11			0.45	−0.08	−6.24	22.76		−15.74
1	2	−9.22	21.00		0.39	−0.03	12.14	12.14	21.00	−8.86
		−9.52			0.32	−0.03	11.78	11.78		−9.22
1	3	−3.35			0.26	0.01	−3.08	−3.08		−3.08
		−3.30			0.22	0.01	−3.07	−3.07		−3.07
1	4	−0.43			−0.06	0.00	−0.49	−0.49		−0.49
		−0.28			−0.04	0.00	−0.32	−0.32		−0.32
2	2	−9.73	−4.50		0.37	0.01	−13.86	43.14	52.50	−9.36
		−9.97			0.31	0.00	−14.15	42.85		−9.65
2	3	−6.16	28.43		0.28	0.02	22.57	22.57	28.43	−5.86
		−6.17			0.24	0.01	22.52	22.52		−5.91
2	4	−2.42			−0.05	0.02	−2.44	−2.44		−2.44
		−2.21			−0.03	0.02	−2.23	−2.23		−2.23
3	3	−6.08	−18.50		0.25	0.00	−24.33	60.67	66.50	−5.83
		−6.06			0.22	0.00	−24.34	60.66		−5.84
3	4	−3.84	35.69		−0.03	0.01	31.83	31.83	35.69	−3.86
		−3.65			−0.03	0.00	32.02	32.02		−3.67
4	4	−3.62	−32.50		0.24	0.02	−35.86	77.14	80.50	−3.36
		−3.37			0.20	0.01	−35.66	77.34		−3.16

consistently for the calculations of the binding energy of ^{16}O, it seems natural to employ the self-consistent selection of E_0^v in the calculation of the binding of ^{17}O with respect to ^{16}O, i.e., for the calculation of the $d_{5/2}$ state in ^{17}O. In this sense, the similar residual dependence on $V_0 - C$ is satisfying. This self-consistent philosophy for E_0^v also is responsible for the V_0 dependence in the SM calculation.

There are two questions that can now be answered with these results. Can a single value of $V_0 - C$ be found to yield approximate agreement with experiment in ^{16}O and ^{17}O? Similarly, can a $V_0 - C$ be found to yield approximate agreement with exp(s) (Ref. 9) results? In both cases the answers are encouraging and the $V_0 - C$ values so found provide further insights into these results.

If we take into account the c.m. correction to E/A which should lower the E/A curve in Fig. 6 by about 0.66 MeV and if we apply the effects of the Coulomb potential which should raise the curve by about 1.13 MeV, we find that $V_0 - C = 48$ MeV yields $E/A \simeq 8$ MeV, which is in good agreement with experiment. As shown in Table III, this choice of $V_0 - C$ results in $E(d_{5/2}) = -2.97$ MeV which is not in such close agreement with experiment (−4.11 MeV), especially when we consider that no c.m. correction has been applied. From the work of

TABLE II. $H_{\text{eff}}(s_{1/2})$. Contributions to the effective Hamiltonian matrix elements for the $s_{1/2}$ states of ^{17}O. Again, the first row of each entry corresponds to an RBSM calculation with $V_0 - C = 48$ MeV but the self-consistent value of E_0^v is −2.2 MeV. The second row gives the SM effective Hamiltonian with $V_0 = 78$ MeV and $C = 30$ MeV while $E_0^v = -3.5$ MeV, the self-consistent choice. See caption to Table I.

n	n'	Diagram								
		G insertion	$-U_0$ insertion	1(b)	1(c)	1($d+e$)	U_{eff}	H_{eff}	T	$\bar{U}_{\text{eff}}$
1	1	−27.96	23.50	0.22	2.44	0.42	−1.39	−0.39	24.50	−24.89
		−28.62		0.21	1.50	0.25	−3.18	−2.18		−26.68
1	2	−13.20	15.65	0.02	1.09	−0.17	3.40	3.40	15.65	−12.25
		−13.80		0.02	0.81	−0.14	2.55	2.55		−13.10
1	3	−3.48		0.00	0.42	0.02	−3.05	−3.05		−3.05
		−3.79		−0.01	0.39	0.02	−3.39	−3.39		−3.39
1	4	−0.28		0.00	0.20	0.22	0.14	0.14		0.14
		−0.37		0.00	0.20	0.15	−0.02	−0.02		−0.02
1	5	0.07		0.00	0.08	−0.05	0.10	0.10		0.10
		0.06		0.00	0.08	−0.03	0.11	0.11		0.11
2	2	−15.81	9.50	0.00	1.28	−0.06	−5.09	23.91	38.50	−14.59
		−16.31		0.00	0.91	−0.06	−5.95	23.05		−15.45
2	3	−9.58	22.68	0.00	0.66	0.03	13.80	13.80	22.68	−8.88
		−9.73		0.00	0.56	0.02	13.53	13.53		−9.15
2	4	−3.68		0.00	0.32	0.05	−3.32	−3.32		−3.32
		−3.60		0.00	0.30	0.03	−3.27	−3.27		−3.27
2	5	−0.85		0.00	0.17	−0.04	−0.71	−0.71		−0.71
		−0.74		0.00	0.17	−0.03	−0.60	−0.60		−0.60
3	3	−10.14	−4.50	0.00	0.68	0.00	−13.95	43.05	52.50	−9.45
		−10.20		0.01	0.58	−0.01	−14.13	42.87		−9.63
3	4	−6.52	29.70	0.00	0.40	0.00	23.58	23.58	29.70	−6.12
		−6.42		0.00	0.36	0.00	23.64	23.64		−6.06
3	5	−2.78		0.00	0.24	0.28	−2.51	−2.51		−2.51
		−2.56		0.00	0.23	0.03	−2.30	−2.30		−2.30
4	4	−6.44	−18.50	0.00	0.39	0.01	−24.54	60.46	66.50	−6.04
		−6.31		0.00	0.36	0.01	−24.44	60.56		−5.94
4	5	−4.17	36.71	0.00	0.28	−0.04	32.77	32.77	36.71	−3.94
		−3.91		0.00	0.26	−0.04	33.02	33.02		−3.69
5	5	−3.93	−32.50	0.00	0.28	−0.02	−36.17	76.83	80.50	−3.67
		−3.61		0.00	0.26	−0.03	−35.88	77.12		−3.38

Krenciglowa and Bando[5] we would estimate the c.m. correction to valence particle energies will provide a repulsive shift of several hundred kilovolts. Thus the $d_{5/2}$ state seems to be underbound by approximately 1.5 MeV.

This underbinding could signal the importance of some neglected diagrams for the valence and/or core processes which cannot be included in the $V_0 - C$ parametrization. However, if we look not only at the $d_{5/2}$ state, but also the $s_{1/2}$ and $d_{3/2}$ states, we note that the overall average agreement is much better. It could be that much of our problem with the $d_{5/2}$ state lies in a lack of spin-orbit splitting—a common problem with microscopic calculations. Overall, the agreement with experiment for the combined ^{16}O and ^{17}O results is remarkably good. Table III displays a capsule summary of E/A, the core and valence single-particle energies, and the core occupation probabilities for $V_0 - C = 48$ MeV. We also present some SM results for comparison.

It is additionally interesting that for $V_0 - C = 48$ MeV, if we choose $V_0 = 63$ and $C = 15$, the positions of the lowest unperturbed levels are $E(s, p, sd) = (-42, -28, +1)$ which are rather close to the final results that emerge. This is pleasing but not necessarily of fundamental significance. However, there is one conclusion relevant to continued valence sd shell studies that can now be made. The self-consistent $d_{5/2}$ is lowered from its unperturbed value by only a small amount—about 4 MeV. This implies that in $A = 18$ there will only be a small gap between the sd shell and the unperturbed pf shell. Thus the $A = 18$ H_{eff} will tend to be very attractive on this score. However, the expected moderating influence of self-consistent $A = 17$ wave functions may well compensate for the small $A = 18$ gap effect so that the $A = 18$ results might

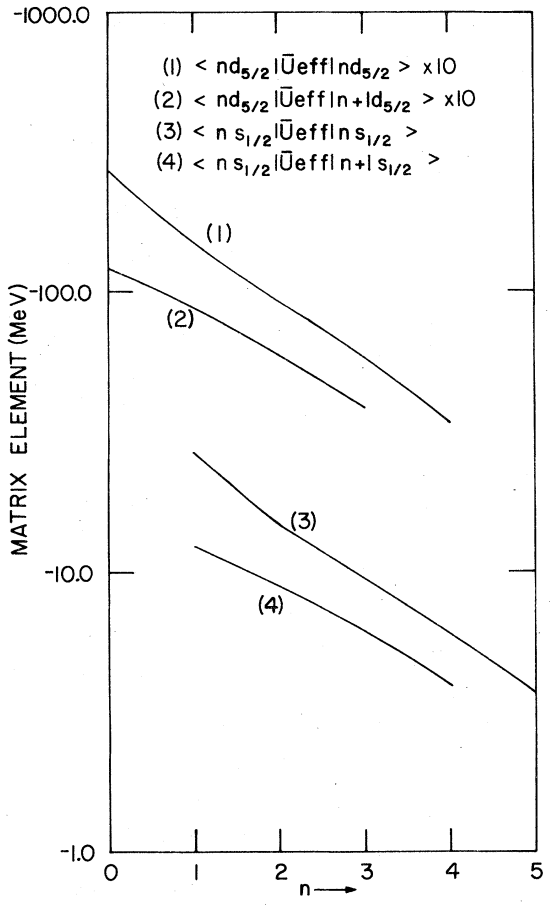

FIG. 5. Logarithmic plot of the diagonal and first off-diagonal matrix elements of the $d_{5/2}$ and $s_{1/2}$ effective single-particle potentials U_{eff} given in Tables I and II respectively. The indicated exponential falloff is used to extrapolate these matrix elements to a 10 major shell basis.

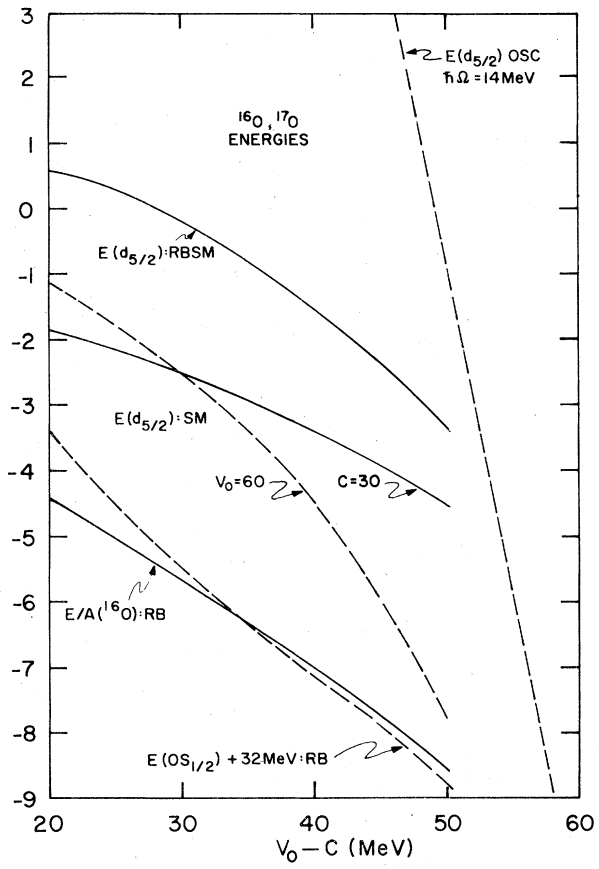

FIG. 6. Selected energies of ^{16}O and ^{17}O as a function of $V_0 - C$. Curves labeled RB refer to the core, SM to a shell-model calculation without introducing the core, and RBSM to our most complete valence calculation. In order to exhibit progress toward convergence we also show the unperturbed $0d_{5/2}$ energy.

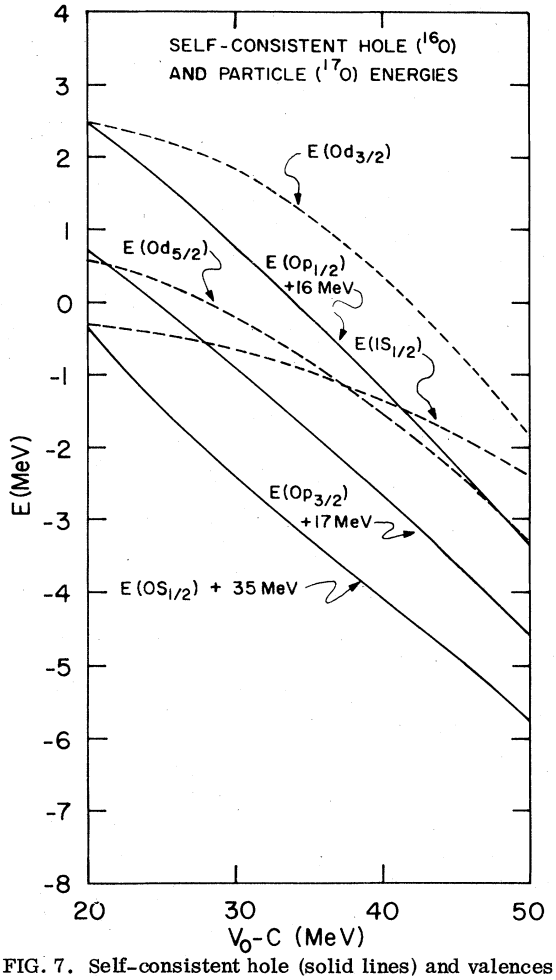

FIG. 7. Self-consistent hole (solid lines) and valences (dashed lines) energies resulting from the RB and RBSM calculations, respectively. The hole energies have been shifted upward to make the similarity in the V_0-C dependence of all self-consistent hole and particle energies readily apparent. Only the $1s_{1/2}$ state, which should be coupled to the $0s_{1/2}$ core state, exhibits a slightly different behavior.

have a net attraction which is quite reasonable.

The other region of interest centers about $V_0-C=33$ MeV where E/A (with estimated c.m. and Coulomb corrections) agrees with the exp(s) results[9] of -5.50 MeV. At this V_0-C value, however, the $d_{5/2}$ state (with c.m. correction) is bound by only a couple of hundred kilovolts. The exp(s) results are also underbound but not nearly by the same amount. This again could signal the importance of some neglected valence diagrams but we already know full convergence is not achieved since some residual V_0-C dependence remains.

In the exp(s) studies it has been noted[10] that a weak attractive potential of $\langle U\rangle\sim-8$ MeV on particle states provides optimal convergence. To achieve this with the *sd* shell would imply lowering the pure oscillator value of 49 MeV first to the average kinetic energy position of 24.5 MeV and then an additional lowering by 8 to 16.5 MeV finally. The total V_0-C is then 24.5 MeV + 8 or 32.5 MeV. It is interesting that this results in the value of V_0-C whereby we achieve, within RB, close agreement with exp(s) for the binding energy of ^{16}O.

In Table III we also summarize the SM and RBSM results for $V_0-C=33$ MeV. In the SM case where there is V_0 dependence due to the self-consistent rather than unperturbed choice of E_0^v, we choose to display the $V_0=59$, $C=26$ results. This is done in order to put the unperturbed $0s_{1/2}$ orbit at -38 MeV, the value it achieves in the RB calculation at the same V_0-C. Incidentally, the SM results for the valence states are then in reasonable accord with experiment.

Figs. 8–10 portray the valence single-particle wave functions that result from the first row of calculations summarized in Table III. In each of these figures we show for comparison the unperturbed harmonic oscillator wave function ($\hbar\Omega=14$ MeV). The overlaps of these oscillator wave functions with the full RBSM results are (0.981, 0.898, 0.945) for the ($d_{5/2}$, $s_{1/2}$, $d_{3/2}$) orbits, respectively. In Figs. 8 and 9 we also display Woods-Saxon wave functions which have been found phenomenologically successful in a recent fit to the ^{16}O(d,p) ^{17}O experiment at three energies.[11] The Woods-Saxon parameters for the $d_{5/2}$ orbit are $V_0=45.099$ MeV, $a=0.4514$ fm, $r_0=1.350$ fm, and $V_{so}=5.517$ MeV. For the $s_{1/2}$ orbit the parameters are V_0

TABLE III. ^{16}O ground state and ^{17}O spectra. Calculated properties of the ground state of ^{16}O in the RB framework and properties of ^{17}O in the RBSM and SM approaches. The unperturbed Hamiltonian is specified by V_0 and C in the SM studies but the ^{16}O and ^{17}O results depend only on V_0-C in the RBSM calculation. Single-particle energies E and occupation probabilities P are presented for the cases in which they are calculated.

V_0-C	BE/A	$E(0s_{1/2}, 0p_{3/2}, 0p_{1/2})$	$P(0s_{1/2}, 0p_{3/2}, 0p_{1/2})$	$E(d_{5/2})$	$E(s_{1/2})$	$E(d_{3/2})$
48	8.30	(−40.5, −21.2, −19.0)	(.83, .84, .83)	−2.97	−2.21	−1.31
48($V_0=78$, $C=30$)		no RB		−4.31	−3.46	−1.33
33	6.11	(−38.0, −18.5, −15.9)	(.86, .87, .86)	−0.52	−0.86	1.45
33($V_0=59$, $C=26$)		no RB		−3.12	−2.58	−0.14

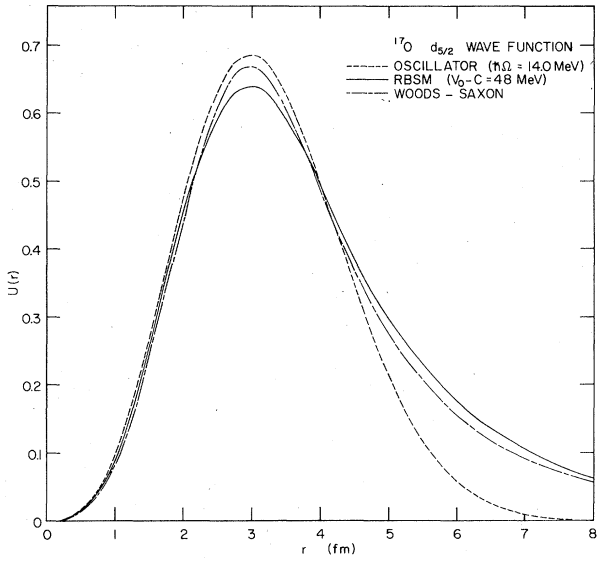

FIG. 8. Wave function for the $d_{5/2}$ state of ^{17}O in the RBSM calculation compared with the harmonic oscillator and Woods-Saxon wave functions. This Woods-Saxon wave function has been shown phenomenologically successful in the recent analysis of (d,p) experiments in Ref. 11.

$=48.672$ MeV, $a=0.4888$ fm, and $r_0=1.300$ fm. Additional Woods-Saxon wave functions were found successful in the analysis of these (d,p) data[11]; however, they all appear very similar to the Woods-Saxon wave functions plotted here. The similarity

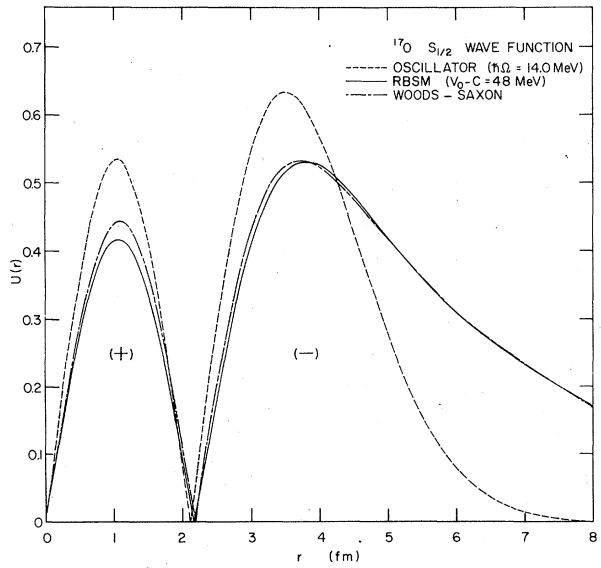

FIG. 9. Wave function for the valence $s_{1/2}$ state of ^{17}O in the RBSM calculation compared with harmonic oscillator and Woods-Saxon wave functions. The Woods-Saxon choice comes from Ref. 11.

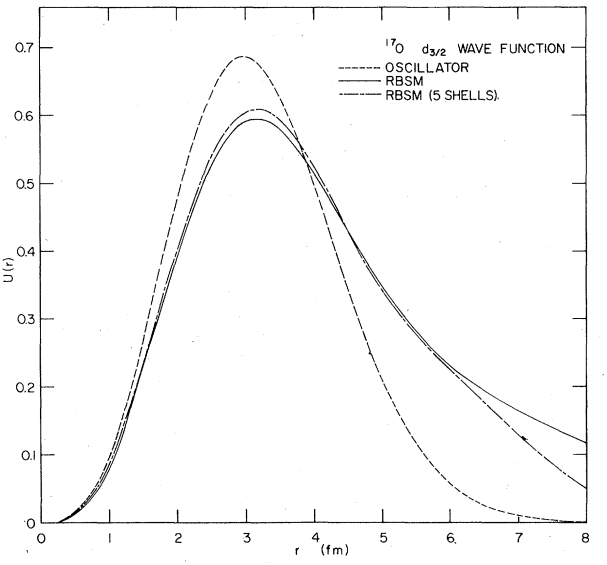

FIG. 10. Wave function for the $d_{3/2}$ state of ^{17}O in the RBSM calculation compared with the harmonic oscillator and with RBSM calculation in only 5 oscillator shells. The solid curve represents the standard full RBSM calculation in 10 oscillator shells with self-consistent E_0^v as described in the text. As in Figs. 8 and 9 the RBSM calculations are done with $V_0 - C = 48$ MeV.

between the phenomenologically successful Woods-Saxon wave functions and the self-consistent RBSM wave functions is an encouraging sign.

In Fig. 10 we compare the $d_{3/2}$ RBSM wave functions obtained by diagonalizing in the 5 shell oscillator space, with that obtained in the full 10 shell diagonalization. The larger space yields an improved exponential tail in the 6 to 8 fm region. This was also observed in the $d_{5/2}$ and $s_{1/2}$ calculations. Between 100 and 200 keV additional binding is obtained by expanding the diagonalization space from 5 to 10 shells. It was found that the SM and RBSM wave functions were very similar when their binding energies were close, so only the RBSM wave functions are shown.

The feature that the self-consistent $A=17$ valence wave functions are pushed out relative to the unperturbed oscillator has been noted in previous studies. It is this feature that plays a major role in reducing the attractive strength of the bare G in $A=18$ calculations. It is obvious from our calculations that large valence spaces are needed to describe the wave functions in the asymptotic region. We plan to use these wave functions in future calculations of the electromagnetic properties of the $A=17$ system.

ACKNOWLEDGMENTS

This work was supported in part by the United States Department of Energy Division of Nuclear Physics and in part by the National Science Foundation under Grant No. Phy78-11628.

APPENDIX: CALCULATIONAL DETAILS

We define for convenience a multiple delta function

$$\Delta_{\beta,\alpha}=\delta(j_\alpha,j_\beta)\delta(l_\alpha,l_\beta)\delta(m_{j_\alpha},m_{j_\beta})\delta(t_{z_\alpha},t_{z_\beta}) \quad \text{(A1)}$$

and the generalized RB single-particle insertion

$$I(\beta,\alpha,E)=\Delta_{\beta,\alpha}\left\{\tfrac{1}{2}\hat{j}_\alpha\sum_{h,J,T}\hat{J}\hat{T}\langle\beta hJT\,|\,G(\omega=E+E_h)\,|\,\alpha hJT\rangle P_h-\beta\,|\,U_0(V_0,C)\,|\,\alpha\right\}, \quad \text{(A2)}$$

where $\hat{j}=(2j+1)$. The contributions of Figs. 1a–1e to H_{eff} can now be given as

$$I(b,a,E_0^v)\,, \quad \text{(A3a)}$$

$$\sum_h\frac{I(b,h,E_0^v+E_h-E_a)I(h,a,E_0^v+E_h-E_b)}{E_0^v+E_h-E_a-E_b}\,, \quad \text{(A3b)}$$

$$\Delta_{b,a}\tfrac{1}{2}\hat{j}_a\sum_{\substack{h_1h_2\\p,J,T}}(1+\delta_{p,\alpha})^{1/2}(1+\delta_{p,b})^{1/2}\hat{J}\hat{T}\times\frac{\langle bpJT\,|\,G(E_0^v+E_{h_1}+E_{h_2}-E_a)\,|\,h_1h_2JT\rangle\langle h_1h_2JT\,|\,G(E_0^v+E_{h_1}+E_{h_2}-E_b)\,|\,apJT\rangle}{E_0^v+E_{h_1}+E_{h_2}-E_p-E_a-E_b}\,, \quad \text{(A3c)}$$

$$\frac{\Delta_{b,a}}{2\hat{j}_a}\sum_{\substack{h,p\\J,T}}\hat{J}\hat{T}\,\frac{\langle bhJT\,|\,G(E_0^v+E_h)\,|\,apJT\rangle I(p,h,E_0^v+E_h-E_a)}{E_0^v+E_h-E_a-E_p}\,. \quad \text{(A3d)}$$

$$\frac{\Delta_{b,a}}{2\hat{j}_a}\sum_{\substack{h,p\\J,T}}\hat{J}\hat{T}\,\frac{\langle bpJT\,|\,G(E_0^v+E_h)|ahJT\rangle I(h,p,E_0^v+E_h-E_b)}{E_0^v+E_h-E_b-E_p}\,. \quad \text{(A3e)}$$

The energy E_0^v in Eq. (A3) is the lowest eigenvalue of the diagonalized H_{eff} for each j and must be determined self-consistently.

In the SM calculations all P_h's are equal to unity and all single-particle energies E_α are defined by $H_0(V_0,C)$. The RBSM calculations determine the hole energies and occupation probabilities from the self-consistent equations[12]

$$E_h=\langle h\,|\,T\,|\,h\rangle+\langle h\,|\,U\,|\,h\rangle\,, \quad \text{(A4)}$$

$$\langle h\,|\,U\,|\,h\rangle=\sum_{h'}\langle hh'\,|\,G(E_h+E_{h'})\,|\,hh'\rangle P_{h'}\,, \quad \text{(A5)}$$

$$P_h=\left\{1-\sum_{h'}\langle hh'|\frac{\partial G(\omega)}{\partial\omega}\,|_{\omega=E_h+E_{h'}}\,|\,hh'\rangle P_{h'}\right\}^{-1}\,, \quad \text{(A6)}$$

and the total binding energy of the core is given by

$$E(^{16}\mathrm{O})=\sum_h\langle h\,|\,T|h\rangle+\tfrac{1}{2}\sum_{h,h'}\langle hh'\,|\,G(E_h+E_{h'})\,|\,hh'\rangle P_hP_{h'}+\sum_h(1-P_h)\langle h\,|\,U\,|\,h\rangle\,. \quad \text{(A7)}$$

Equations (A4)–(A6) are solved by iteration, after choosing initial guesses for the hole energies. The reaction matrix elements are calculated on an ω mesh and self-consistent values are obtained at each iteration by interpolation.

A similar self-consistent calculation is carried out for $A=17$. The $d_{5/2}$, $s_{1/2}$, and $d_{3/2}$ calculations must be performed as a function of E_0^v and the resulting eigenvalue iterated until separate convergence is obtained for each j value. It should be emphasized that *only* the lowest eigenstate for each j is treated self-consistently.

*Permanent address.
[1]C. Bloch and J. Horowitz, Nucl. Phys. 8, 91 (1958); B. H. Brandow, Rev. Mod. Phys. 39, 771 (1967); J. F. Dawson, I. Talmi, and J. D. Waleeka, Ann. Phys. (N.Y.) 18, 339 (1962); G. F. Bertsch, Nucl. Phys. 74, 234 (1965); T. T. S. Kuo and G. E. Brown, *ibid.* 85, 40 (1966).
[2]B. R. Barrett and M. W. Kirson, Nucl. Phys. A148, 145 (1970).
[3]J. P. Vary, P. U. Sauer, and C. W. Wong, Phys. Rev. C 7, 1776 (1973); C. L. Kung, T. T. S. Kuo, and K. F. Ratcliff, *ibid.* 19, 1063 (1979).
[4]P. J. Ellis and H. A. Mavromatis, Nucl. Phys. A175, 309 (1971); P. J. Ellis and E. Osnes, Phys. Lett. 41B, 97 (1972); H. N. Comins and R. G. L. Hewitt, Nucl. Phys. A228, 141 (1974); A228, 153 (1974); Y. Stark- and and M. W. Kirson, *ibid.*, A261, 453 (1976); J. Shurpin, H. Müther, T. T. S. Kuo, and A. Faessler, *ibid.* A293, 61 (1977).
[5]E. M. Krenciglowa and H. Bando, Nucl. Phys. A294, 191 (1978).
[6]N. I. Kassis, Nucl. Phys. A194, 205 (1972).
[7]J. P. Vary and S. N. Yang, Phys. Rev. C 15, 1545 (1977).
[8]K. T. R. Davies and R. J. McCarthy, Phys. Rev. C 4, 81 (1971).
[9]H. Kümmel, K. H. Lurhmann, and J. G. Zabolitsky, Phys. Rep. 36C, 1 (1978).
[10]J. G. Zabolitsky, Phys. Rev. C 14, 1207 (1976).
[11]M. D. Cooper, W. F. Hornyak, and P. G. Roos, Nucl. Phys. A218, 249 (1974).
[12]R. J. McCarthy and K. T. R. Davies, Phys. Rev. C 1, 1644 (1970); B. R. Barrett, R. G. L. Hewitt, and R. J. McCarthy, Nucl. Phys. A184, 13 (1972).